ATOMIC STRUCTURE AND PHYSICAL PROPERTIES OF CRYSTALS

V. I. SIMONOV

Institute of Crystallography, USSR Acad. Sci., Moscow

The relation between the structure and physical properties of crystals can be determined on the basis of precisional structural investigations. Of major importance in such studies is not only a highly accurate determination of atomic coordinates, but also reliable determination of their thermal motion parameters with account of anisotropy and anharmonism of atomic thermal vibrations. If an investigator is primarily interested in the character of chemical bonding in crystals and molecules, then the structural study will be aimed at the construction and analysis of deformation electron density in the crystal under study:

$$\delta\rho(r) = \rho(r) - \Sigma\, \rho_i\, (r - r_i) \qquad (1)$$

where $\rho(r)$ is electron density distribution, $\Sigma\rho_i\,(r - r_i)$ is a superposition of spherically symmetric densities of free (not envolved in chemical bonding) atoms of the given crystal. Of course, many physical properties of crystalline materials are accounted for not only by the atomic (ideal) but also by a real crystal structure. This report is devoted mainly to X-ray and neutron diffraction studies of the atomic structure of single crystals. Crystalline materials exhibit significant changes of their physical properties during phase transitions. Methods of X-ray structural studies provide for a unique possibility of studying the atomic mechanisms of phase transitions in crystals. To do this it is necessary to conduct diffraction experiments under the influence of external actions (such as temperatures, pressures, electronic field, etc.) on the sample.

Accurate structural investigations have become possible as soon as computer-controlled four-circle diffractometers were developed. These apparatus permit optimization of the measurements of reflection intensi-

ties using feed-back at the level of each reflection. Futher advances in diffraction experimental techniques allow one to obtain reproducible results of measurements of integral intensities to an accuracy of 1-3%. Advances in the theory of the interaction of radiation with crystals permits one to take into account all the effects of such interaction while calculating reflection intensities into moduli of structure amplitudes. First of all, an account should be made of the geometry of intensity measurement, background, radiation polarization and absorption. Then, there are more subtle effects of interaction, some of them can be taken into account only at final stages of the study, during least squares refinement of the model. These are extinction, thermal diffuse scattering, simultaneous reflections and other more fine effects between the radiation and substance.

The analysis of data in the literature and our experience in that field suggest that a formal application of the available program systems does not always yield physically meaningful structure parameters. It concerns not only the measurements accuracy and data processing. There may be a strong correlation between structure parameters. In fact, there is almost always a correlation between the coefficient of reduction of the observed structure amplitudes to an absolute scale and the parameter of atomic thermal motion. The situation becomes still more complicated if there are significant extinction effects. The structures with statistical replacement of sites by some atoms exhibit a strong correlation between site occupancies and parameters of thermal motion of such atoms. Also hazardous is the correlation in the case when atoms occupy statistically the sites that are split into two or more close positions. In case there are remarkable correlations, the appropriate confidence intervals should be constructed for all correlating parameters. The parameter values and error estimations should be considered only with an account of these confidence intervals. Formally, standard deviations obtained using the least squares technique cannot serve for a reliable estimation of the accuracy of the strongly correlating structure parameters.[1]

Atomic structure and the superconducting transition temperature of (La, Sr)$_2$CuO$_4$

High-temperature superconductivity was discovered on ceramic samples of (La, Ba)$_2$CuO$_4$.[2] Then, during three years all the attempts to obtain single crystals of La-phases with T_c = 36 K, that is typical of the best ceramic materials, were unsuccesful. In the first year after the discovery of high-temperature superconductivity single crystals of (La, Sr)$_2$CuO$_4$ with T_c = 5–10 K were obtained. A year later single crystals with T_c = 17 K and

then, 24 K, were obtained. It is only in recent times that single crystals with T_c = 30 K, that is the temperature of ceramic samples have been obtained. A dependence of T_c on Sr content in $(La, Sr)_2CuO_4$ was established for ceramic materials. As for crystalline materials, such an unambiguous dependence was not found. There were samples with identical Sr contents and essentially different superconducting transition temperatures. Our structural studies of single crystals with Sr content ranging from $(La_{0.97}\ Sr_{0.03})_2CuO_{4-\delta}$ to $(La_{0.88}\ Sr_{0.12})_2\ CuO_{4-\delta}$ permitted us to find reasons why there is no regular T_c dependence on Sr content in single crystals.

Precision structural studies of crystals of La-phases are hindered due to twinning. The analysis of only ϑ-profiles of reflections often does not provide an unambiguous solution of the question whether there is twinning in particular samples. Twinning and its character can be reliably established by means of two-dimensional $\omega/2\vartheta$ scanning of reflections. Fig. 1 presents one-dimensional ϑ-profiles and two-dimensional $\omega/2\vartheta$ scans of (10 2 0) and (2 10 0) reflections from a twin $(La_{0.97}\ Sr_{0.03})_2CuO_{4-\delta}$. All the samples studied exhibited twinning over (1 1 0) or (1 $\bar{1}$ 0) planes. Twin volume ratios in different samples varied from 1:1 to 1:0.45. The analysis of the symmetry with account of twinning showed that all the samples belong to two centrosymmetric orthorhombic space groups Abma and Pbma. A centered Bravais lattice characterizes crystals with low Sr content. For samples with a higher Sr content we have reliably established reflections that disturb the A centering. The space group in this case is Pbma.

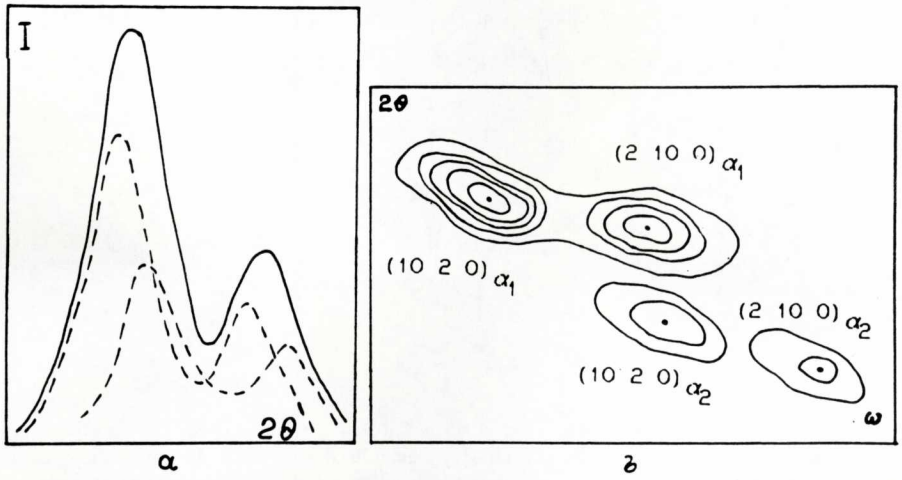

Fig. 1. a) Observed (solid line) and split (dashed lines) ϑ-profiles of (10 2 0) and (2 10 0) reflections of $(La_{0.97}\ Sr_{0.03})_2\ CuO_{4-\delta}$ crystal. b) Two-dimensional scan of the same reflections.

A principle difference between crystals belonging to different space groups, as far as their structure is concerned, consists in the fact that there is only one crystallographically independent La atom in the independent part of a centred unit cell. If we take space group Pbma with a primitive Bravais lattice there are two independent La atoms in the structure. A physical difference between these two structural types consists in the fact that Sr atoms are distributed statistically uniformly over all La sites in crystals with space group Abma. In the case of crystals with a primitive Bravais lattice we have found partial or full order in Sr distribution over La sites[3, 4]. Fig. 2 presents atomic models of three structures with various Sr distribution over La sites. In crystals $(La_{0.97}\ Sr_{0.03})_2\ CuO_{4-\delta}$ La is replaced by Sr at any La site with equal probabilily. In crystals of $(La_{0.94}\ Sr_{0.06})\ (La_{0.86}\ Sr_{0.14})\ CuO_{4-\delta}$ there is partial order in Sr distribution over La sites. The probabilily of Sr atom occupation of La site is 6%, while the probability of the occupation of the second La site is 14%. And, finally, we have established full order in Sr distribution in La $(La_{0.76}\ Sr_{0.24})CuO_{3.92}$. In this case one crystallographic site is 100% La occupied, all Sr atoms are concentrated at the second La site. At the latter site La is replaced by Sr with a probability of 24%. We see in Fig. 2 that in the case of fully ordered

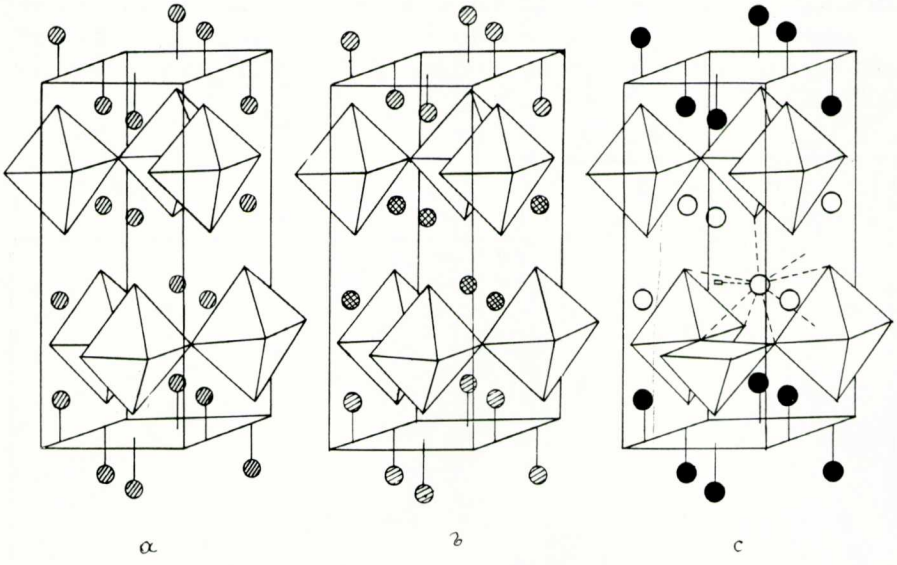

Fig. 2. Models of the atomic structure of $(La,Sr)_2\ CuO_{4-\delta}$ crystals with various Sr atom distribution over La sites. a) $(La_{0.97}\ Sr_{0.03})_2\ CuO_{4-\delta}$ – even Sr atom distribution over all La sites. b) $(La_{0.94}\ Sr_{0.06})\ (La_{0.86}\ Sr_{0.14})\ CuO_{4-\delta}$ – partial order in Sr atom distribution. c) La $(La_{0.76}\ Sr_{0.24})$ $CuO_{3,92}$ –full order, Sr atoms replace La only at one of its sites. Sr concentration in double layers of the structure leads to oxygen deficiency in these layers.

Sr distribution strontium is concentrated in double layers between layers of Cu-octahedra. A direct result of replacement of trivalent La atoms by divalent Sr atoms when the latter are concentrated in localized double layers is a deficiency in positive valence forces in these layers. As a result, some O atoms from parts of the structure enriched with Sr, leave the crystal. Accurate structural studies allowed us to establish reliably the oxygen deficiency in such layers where all Sr atoms are concentrated (Fig. 2c). Neutron diffraction studies[5] have shown that in $La_2CuO_{4.032}$ crystals the compound neutrality is ensured by the formation of $[O_2]^{2-}$ groups with O-O distance 1.64 Å. Supposedly, in our case the formation of such groups compensates for La replacement by Sr only if Sr atoms are evenly distributed over all La sites. When Sr atoms are ordered and contained at certain layers of the structure there occur some oxygen atom losses in the structure. This, in its turn, affects the physical properties of crystals and leads to a lowering of T_c.

Our results concerning the ordered Sr atom distribution when Sr atoms replace La atoms suggest two conclusions. 1. The T_c of $(La, Sr)_2CuO_{4-\delta}$ crystals depends not only on Sr content in the sample but also on Sr atom distribution over La sites. 2. The differences in the properties of single crystals and ceramic materials when Sr content in them is the same are due to differences in Sr atom distribution. The techniques of growing single crystals are closer to equilibrum ones as compared to ceramics. That is why the probability of Sr order is higher in single crystals. In ceramics an even Sr atom distribution and the formation of $[O_2]^{2-}$ groups without O losses is more probable. This result gives us higher T_c in ceramics as compared to single crystals with a fixed total Sr content.

Atomic Structure and T_c of Y-phases of High-Temperature Superconductors with Various Oxygen Content

Accurate structural studies of $YBa_2Cu_3O_{7-\delta}$ single crystals with O content ranging from 6.24 to 6.97 per unit cell have been carried out. The oxygen content was varied by dozaged annealing in an argon atmosphere according to[6]. All the studied samples were, in fact, twins with (1 1 0) and (1 $\bar{1}$ 0) twinning planes. Two-dimensional $\omega/2\vartheta$ scanning of reflections enable separate estimation of intensities of reflections from different domains of twins. According to these data twin volume ratios and unit cell parameters of single-domain regions were found. The data on the latter are presented in Table 1. In those crystals where oxygen content is lower than 6.5 atoms per unit cell there are regions of local tetragonal symmetry. The lower is O content the larger is the relative volume of tetragonal symmetry

regions with respect to the volume of orthorombic symmetry regions. The refinement of atomic models of these structures was complicated due to a stong correlation between structure parameters. For instance, thermal parameters of O atoms (1/2 0 z) and (0 1/2 z) could be refined only in supposition of equality of these parameters. There was rather a strong correlation for O atom (0 1/2 0) between its temperature factor and the coefficient q of this atom's occupation of its site. The main results obtained in the studies of Y-phases with various oxygen content are best illustrated by changes in one-dimensional ϑ-profiles of (4 0 0) and (0 4 0) reflections from $YBa_2Cu_3O_{7-\delta}$ twins with various O content that we studied.

In the crystal with 6.95 oxygen atoms per unit cell the reflections from different twin domains are practically fully resolved. Integral intensities of these reflections are readily measured because they do not overlap. However, they can be easily approximated by measuring distances and relative intensities from twin domains. (4 0 0) and (0 4 0) reflection profiles for crystals with 6.46 and especially 6.24 oxygen atoms cannot be interpreted so easily by superimposing on one another the reflections

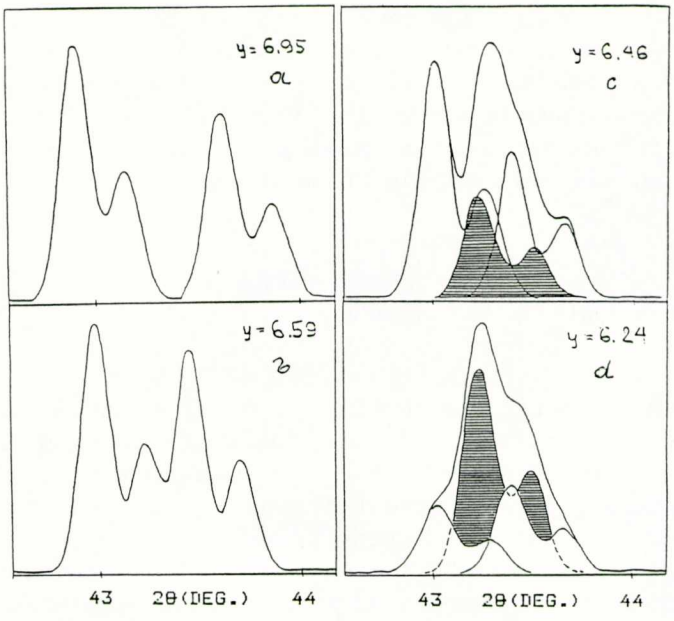

Fig. 3. (400) and (040) reflection profiles of $YBa_2Cu_3O_{7-\delta}$ crystals with various oxygen content: a) 6.95; b) 6.59; c) 6.46; d) 6.24. Components of the scattering by tetragonal regions are shaded.

from orthorhombic twin domains. These complex profiles could be interpreted only by the superposition of the scattering from regions of local tetragonal symmetry. Thus, it was found that there is order in oxygen atom distribution in the sample which we regarded as a single crystal. This order results in the appearance of three types of regions rather large in size, that have different local symmetry. Two types are the orthorhombic twin domains, and the third one is tetragonal symmetry regions. We see from Table 1 that these regions are characterized by different unit cell parameters. Such a difference is best manifested in a sample with 6.24 oxygen atoms. As is well known from the literature, there is a correlation between oxygen content in a sample of 1-2-3 phase and the period of this phase. Thus, we can assume that the regions differing in symmetry unit cell parameters have different composition (namely, oxygen content). We have determined mean oxygen content in the sample from statistical O atom site occupancies. According to the unit cell volume of tetragonal symmetry regions, the composition of these regions can be considered as $YBa_2Cu_3O_6$, from crystal chemical considerations. The volume ratio of tetragonal and orthorhombic regions is calculated from reflection intensities. These data taken as a whole are sufficient to determine the local chemical composition of orthorhombic symmetry regions. In our case for a crystal with mean oxygen content 6.24 the estimation of the local chemical composition of orthorhombic regions yields 6.56 oxygen atoms per unit cell. Within the accuracy of our X-ray data this value is in good agreement with the composition of so-called orthorhombic phase II $YBa_2Cu_3O_{6.5}$, to which a superconducting phase transition at $T_c \sim 60$ K is related.

Thus, on the whole, for the thermodynamically equilibrium crystals of Y-phases the structures of compounds with different oxygen content can be regarded as follows. A strictly tetragonal phase does not undergo a superconducting phase transition and has the chemical composition $YBa_2Cu_3O_6$. If such a crystal is enriched with oxygen, the –Cu–O–Cu–O– chains appear in the plane of Cu atoms. Each such chain alternates with a –Cu–Cu– –chain. Thus, an orthorhombic phase II with $T_c \sim 60$ K is formed, with the local chemical composition $YBa_2Cu_3O_{6.5}$. With an increase in oxygen content the relative value of this phase as compared to the initial tetragonal phase $YBa_2Cu_3O_6$ is also increased.The crystal with the mean total oxygen content 6.5 atoms per unit cell, is fully composed of phase II and undergoes a superconducting phase transition at $T_c \sim 60$ K. A futher increase in oxygen content results in the apperance of an orthorhombic $YBa_2Cu_3O_7$ phase with $T_c \sim 90$ K. Superconductivity (resistance fall) in the entire sample takes place when regions of orthorhombic phases of $YBa_2Cu_3O_7$ become connected. The connection of structure blocks with different oxygen content is shown in Fig. 4. Our patterns of equili-

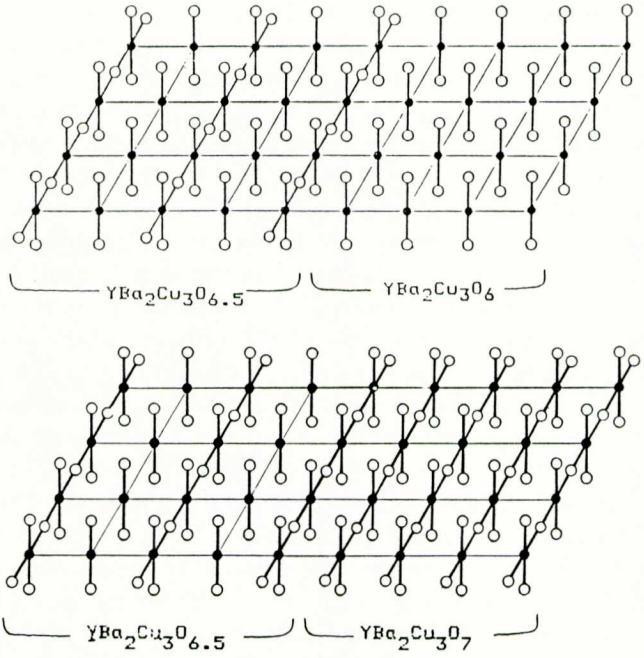

Fig. 4. Connections of YBa_2 Cu_3 O_6 and YBa_2 Cu_3 $O_{6.5}$ blocks in structures containing 6-6.5 O atoms per unit cell (a). Connection of YBa_2 Cu_3 $O_{6.5}$ and YBa_2 Cu_3 O_7 blocks in structures with O content 6.5 – 7 atoms per unit cell(b).

brium atomic structure of $YBa_2Cu_3O_{7-\delta}$ crystals with different oxygen content[7] were later confirmed by electron microscopy studies of Y-phases.[8]

Atomic Structure and Ionic Conductivity of Solid Electrolytes

Crystalline materials with high ionic conductivity attract the attention of investigators because of a diversity of their physical properties and phase transitions in them. The scope of the practical application of solid electrolytes is constantly widening. The most well known superionic conductor on which sodium-sulphuric batteries are based, is β-alumina with the ideal structure 11 $Al_2O_3 - Na_2O$. The non-stoichiometric fluorite-type phases that are the subject matter of the majority of reports made at this seminar, also belong to the class of materials with high anionic conductivity. A specific feature of solid electrolytes is the fact that they can have one–, two– or three– dimensional conductivity. This can be illustrated by

an example of Na_x (Ti, Mg)$_2$ (O, F)$_4$ compound. One-dimensional conductivity along the c axis attains 10^{-2} Ohm^{-1} cm^{-1} at T = 670 K, while in the ab plane the crystal is a dielectric. In this case the one-dimensional conductivity is due to Na^{1+} ion transport along channels composed of (Ti, Mg)-octahedra. The two-dimensional conductivity is typical of the above β-alumina whose atomic structure is layered. Nonstoichiometric fluorite-type phases having cubic symmetry are, of course, three-dimensional conductors.

Let us consider in more detail the structural features and phase transitions to the superionic state of isostructural Li-solid electrolytes $Li_3Sc_2(PO_4)_3$ and $Li_3Fe_2(PO_4)_3$. The establishment of atomic mechanisms of phase transitions in these compounds is hindered by microtwinning in their low-temperature phases. When the crystals are in the superionic conductivity state they have orthorhombic symmetry with a unambiguously determined space group Pcan[9]. Below the superconducting phase transition point the crystals are monoclinic, sp. gr. $P2_1/n$ with a vivid pseudorhombicity. The symmetry elements that are to be lost in this case become elements of pseudosymmetry. The dependence of the violation of the orthorhombic symmetry in the low-temperature phase on the specimen and its history, found from X-ray diffraction data, leads to a variation of the discrepancy in the values of $F(hkl)_{obs}$ and $F(\bar{h}kl)_{obs}$ over a wide range, including even their equality. Detailed structural studies enabled us to find a reason for such irreproducibility of results on passing from one specimen to another and even for one specimen after thermal treatment. This reason was twinning of the specimens and a change in the twin volume ratio. The interpretation of this pattern of microtwinning according to X-ray diffraction data was rather a complicated task. The diffraction patterns from different twinned components were practically completely superimposed upon one another, due to twinning by pseudomerohedry. The reflection peaks were not split, but slightly broadened. A true evidence of twinning were the insignificant (to 1.2′) changes in the angle of unit cell monoclinicity that depended on the ratio of the volumes of the twinned components. For instance, for one of the samples, $Li_3Fe_2(PO_4)_3$, this ratio initially was 1:7.5, but after annealing at 700° C during five hours it changed to 1:1.2.

A correct allowance for twinning during our structural studies enabled us to establish atomic mechanisms of phase transitions in these crystals, as well as to determine the pathway of Li ion transport during the process of the conductivity, and changes in Li atom distribution over their sites at different temperatures. We also found deviations from the law of harmonicity in thermal vibrations of ions involved in charge transport. In full accordance with physical changes, two phase transitions were found in

the studied Li-solid electrolytes from the structural data[10]. Phase transformations in $Li_3Sc_2(PO_4)_3$ and $Li_3Fe_2(PO_4)_3$ crystals are similar. The basis of the atomic structure of these crystals is a three-dimensional framework built of P– tetrahedra and M-octahedra linked via common oxygen vertices. Li atoms that are responsible for a high ionic conductivity in these materials, are located at the voids of a mixed framework. In the low-temperature α-phase 12 lithium atoms fully occupy three crystallographic sites with multiplicities equal to 4. Li1 cations are located at rather regular oxygen tetrahedra. Coordination polyhedra of Li2 and Li3 atoms are distorted trigonal bipyramids. The first phase transition form α-to β-modification occurs without changing the monoclinic space group $P2_1/n$. In this case the structure framework acquires some symmetry features. The main changes during this phase transition occur in the arrangement of Li atoms. The Li 3 atom of α-phase occupies a new site in β-phase, now it is located in an oxygen tetrahedron that is related to Li1 tetrahedron by a new element of orthorhombic symmetry in the superionic γ-phase. The Li atom arrangement in three phases of the $Li_3M_2(PO_4)_3$ structure is schematically presented in Fig. 5.

A peculiar feature of rather diffuse phase transitions consists in the temperature dependence of these transitions $\alpha \rightleftarrows \beta \rightleftarrows \gamma$ on a concrete spe-

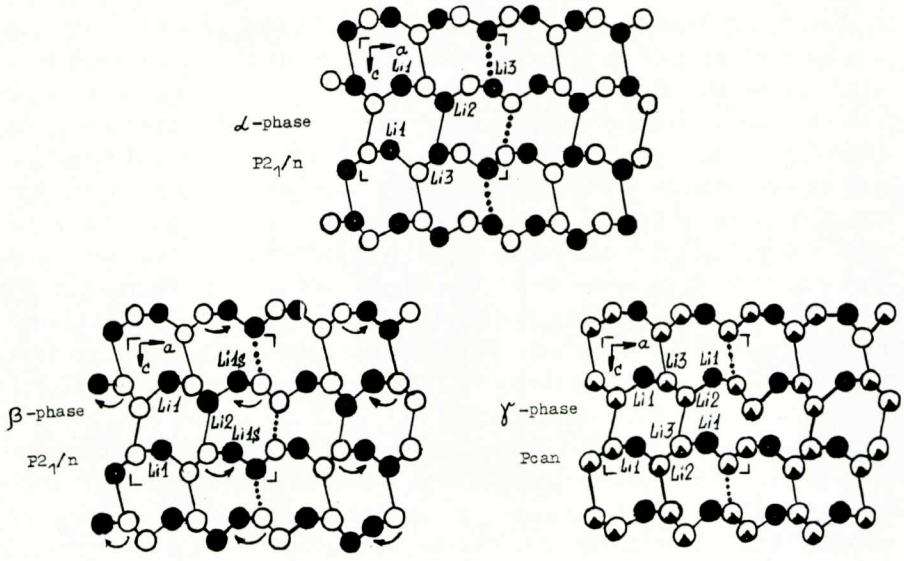

Fig. 5. Schematic arrangement of Li atoms in α–, β– and γ– phases of $Li_3\ M_2\ (PO_4)_3$. Occupied Li atom sites are dark. The black sector denotes partial occupation of a particular site by Li atom.

cimen. Different authors in their works report totally different temperatures of the first and second phase transitions: $\alpha \rightleftharpoons \beta \rightleftharpoons \gamma$ 514 K and 538 K, 450 K and 560 K; 420 K and 516 K. The atomic mechanism of structural transformations enables one to understand the dependence of phase transition temperatures on the sample and its history. The twinning of α– and β– phases, structure inhomogeneities in different parts of the specimen bulk and, finally, a coexistence of α– and β– or β– and γ–phases in the specimen simultaneously makes the phase-transitions diffuse and shifts the mean temperature of these transitions. In the high-temperature γ–phase that possesses a high ionic conductivity, the symmetrization of the structure framework is completed within the framework of space group Pcan. In this case 12 Li atoms are distributed over eight sites with multiplicity equal to 8 within orthorhombic space group. Only the Li 1 atom site is 100% occupied. The probability of lithium atom being located at the other two sites is only 25%. It is these sites that ensure the superionic character of high-temperature γ–phases.

Structural Transition in Se-containing Ferroelectrics.

In most Se-containing compounds the ferroelectric features and mechanisms of phase transitions are due to the character of hydrogen bonds and their changes. Of major importance for the structural studies of such crystals is a reliable localization of hydrogen atoms. Here neutron diffraction techniques should be given preference over X-ray structure analysis. The second specific feature of the studies of ferroelectric phases is the necessity of analyzing diffraction data from crystals divided into ferroelectric domains. In other words, while investigating such objects one should utilize techniques of studying twinned crystals, just like in the case of fast ionic conductors. Let us consider, as an example, the changes in the atomic structure during the transition from the paraelectric to the ferroelectric phase in $RbHSeO_4$[11]. The phase transition takes place at $T_c = 370.5$ K. The paraphase of these crystals contains two crystallographically independent hydrogen bonds. After the protons envolved in these bonds were localized using neutron diffraction techniques, nuclear density distribution maps, in fact, differed significantly from one another near these two bonds (Fig. 6). In one case there is a spherically symmetric extremum corresponding to a fixed position of H(2) atom. The appropriate hydrogen bond has a conventional geometry O(5) – H(2) . . . O(3'), that is not changed during the ferroelectric phase transition. Nuclear density distribution near the H(1) atom is more complex and can be interpreted using two different models. There are the first model of statistical disorder in H(1) atom distribution,

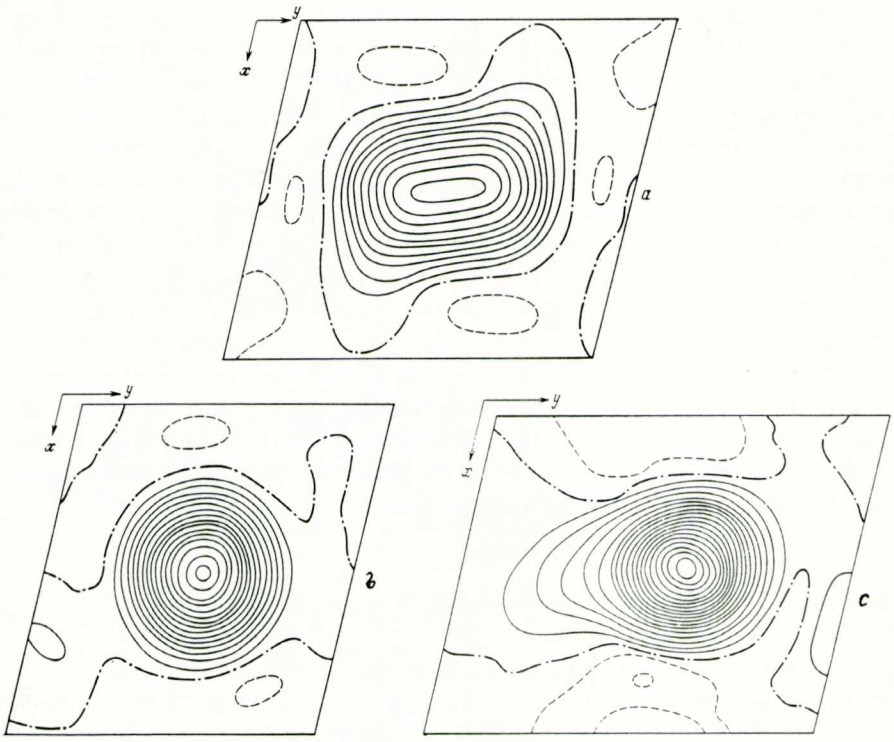

Fig. 6. Nuclear density distribution near H atoms in $RbHSeO_4$: H (1) atom (a), H(2) (b) in paraelectric phase, H(1) atom (c) in ferroelectric phase. The nuclear density distribution for H(2) atom is similar to that in paraelectric phase.

and, the second model, that has a dynamic character. Here, the H(1) atom is located at a middle point of the O(1) – O(1') interval and performs essentially anisotropic thermal vibrations that show deviations from the harmonic law. It is rather difficult to make a choice of these two models directly from diffraction data. According to NMR data a potential relief corresponding to this hydrogen bond has two minima lying symmetrically relative to the middle point on the bond. These minima are statistically occupied by H(1) atoms with equal probabilities. The NMR data evidence hoppings that protons perform between these two minima with a frequency of 10^5 Hz. The time of proton location at a minimum is much longer than the time of a hopping. Such is a full pattern of structural features of a paraelectric phase of $RbHSeO_4$ crystals. Upon the transition to a ferroelectric phase the character of this hydrogen bond differs significantly. Fig. 6c presents nuclear density map near the H(1) atom in the ferrolectric

phase. This pattern can be intepreted in the following way: upon the transition to the ferroelectric phase H(1) atoms envolved in hydrogen bonds become ordered. In this case a single crystal in the ferroelectric phase is split into domains, domain volume ratio being 7.4:1.0. The presence of ferroelectric domains related by two-fold symmetry axis that used to be a crystallographic symmetry axis in the paraelectric phase, is manifested in the asymmetry of the peak of nuclear density distribution for a proton of H(1) atom (Fig. 6c).

The second object of our studies were $Rb_3H(SeO_4)_2$ crystals that undergo two phase transitions at 449 K and 606 K.[12] Below 449 K this is a ferroelectric phase with a typical pattern of crystal spliting into domains, differing in their orientation by 120°. Above 449 K this is a superionic phase with the conductivity 10^{-3} Ohm^{-1} cm^{-1}, typical of solid electrolytes. This compound was studied using X–ray diffraction data. The space groups are as follows: A2/a for the low-temperature phase and R3m for the second one. A specific feature of the atomic structure of the superionic phase of $Rb_3H(SeO_4)_2$ is disorder in the distribution of one oxygen vertex of Se-tetrahedron along the three-fold axis. As a result, a statistical two-dimentional network of hydrogen bonds is formed in the plane perpendicular to the three-fold axis (Fig. 7). The probability of realization of each of this network is 1/3. It is this disorder that accounts for a high protonic conductivity of the phase. Upon the transition to the low-temperature phase there is order in O atom distribution and domains having three orientations rotated through 120° relative to one another, are formed in the crystal.

While studying $(NH_4)_2Se_2O_5$ crystals we have found that the phase transition at T = 312 K occurs without changing the space group $P2_12_12_1$. The atomic mechanism of the phase transition consists in the mutual rotation of $[Se_2O_5]$ and $[NH_4]$ groups of atoms. One hydrogen bond is ruptured and another hydrogen bond is formed. The structural study was carried out on single crystals using neutron diffraction techniques.

Anharmonic Thermal Vibrations of Atoms in Acoustooptical Single Crystals of α-TeO_2

Unique acoustooptical properties of single crystals of paratellurite make it an interesting object for studies[13]. It is the slow transverse acoustic wave propagating in [1 1 0] direction with [1 $\bar{1}$ 0] polarization that is used in practice[14]. This acoustic mode is characterized by rather high absorption coefficient – 290dB/cm at a frequency 1 ГHz, that exceeds the absorption coefficient of elastic ultrasonic waves in α-TeO_2 by two orders

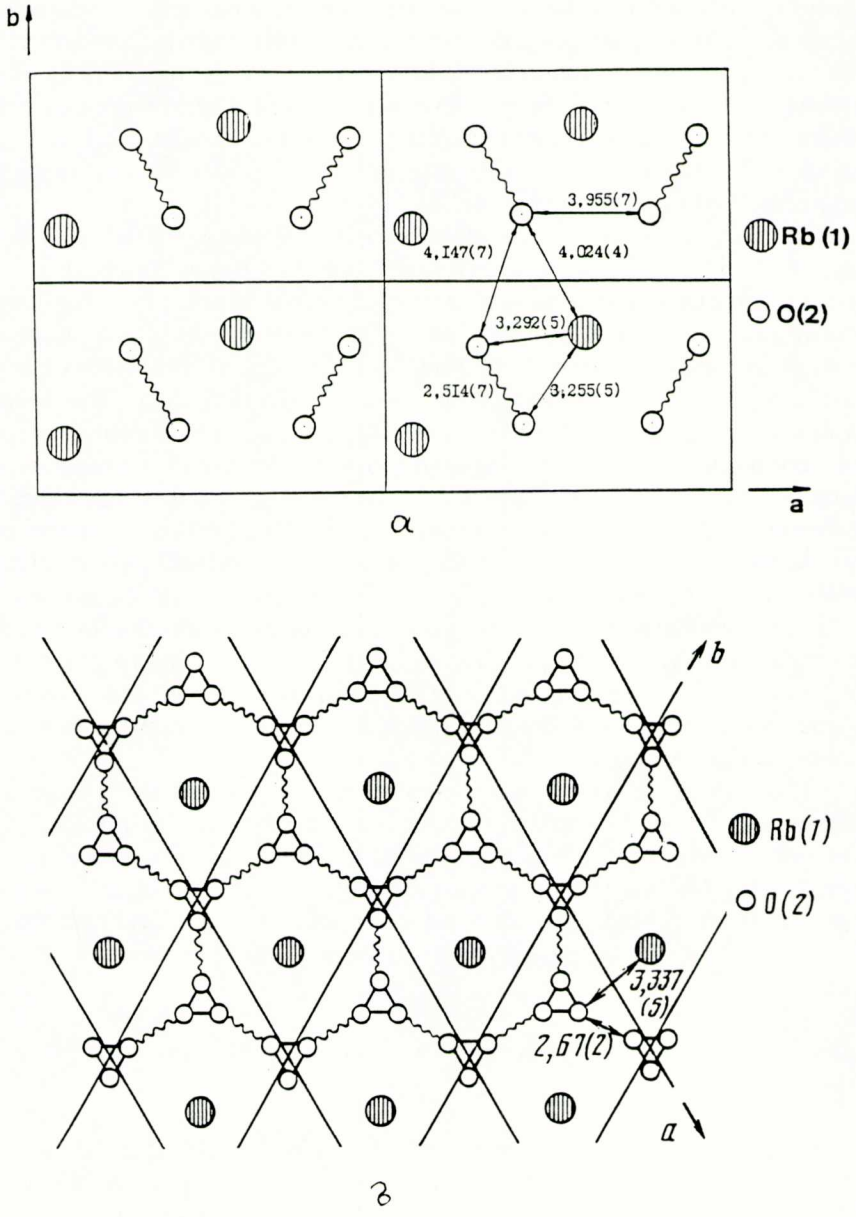

Fig. 7. A fragment of the structure of $Rb_3H(SeO_4)_2$ in paraphase (a) and in the superionic phase (b). Wavy line denotes hydrogen bonds, ordered (a) and statistical (b).

of magnitude. It is this circumstance that has stimulated our studies of anharmonicity of thermal vibrations of atoms in paratellurite[15]. The study was performed from X-ray diffraction data on single crystals. A total of 7167 reflectons were measured in the reciprocal space using MoK_α-radiation. An array of 844 moduli of independent structural amplitudies was obtained after averaging over equivalent reflections with account of the tetragonal symmetry a =4.810(1) and c = 7.613(2) Å. By making use of anomalous dispersion effect, an absolute configuration of the single crystals studied was established, sp.gr. $p4_32_12$. The final discrepancy indices were R = 0.88 and R_w = 1.16%. We managed to reduce them down only to 1.40 and 1.74% for enantiomorphic group $P4_12_12$. We used the technique of the refinement of structure parameters with high values of sin ϑ/λ for the observed structure amplitudes to establish anharmonicity of thermal vibrations of atoms and to locate a lone electron pair of Te atom.

The anharmonicity of thermal vibrations of Te and O atoms is determined using Gram-Charlier formalism[16] with allowance for anharmonicity of corrections up to the 6-th rank. According to our X-ray diffraction data only two independent coefficients C^{111} and C^{112} of third-rank tensor are significant for Te atoms. Fig. 8 shows a section of anharmonic component of the probability density distribution of Te atom location at a given point

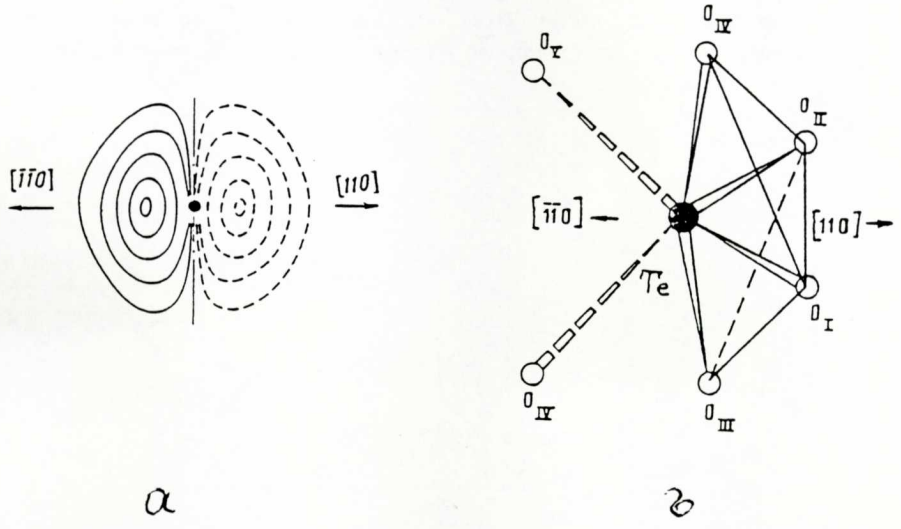

Fig. 8. Structure of α-TeO_2. Section of the anharmonic component of probability density function of Te atom location at a certain point (a). The closest environment of Te by O atoms (b).

of space in the process of thermal vibrations. This figure also shows the closest oxygen environment of Te atoms. It is evident from the geometry of this structure fragment that Te atom displacement along the [1 1 0] direction results in a reduction of Te-O bonds for all oxygen atoms of the first coordination sphere. Tellurium atom displacement in the [$\bar{1}$ $\bar{1}$ 0] direction results in an increase of all these distances. This is a reason of remarkably asymmetric single-atom Te atom potential in opposite [1 1 0] and [$\bar{1}$ $\bar{1}$ 0] directions.

As mentioned above, the maximum acoustic wave absorption 290 dB/cm in α-TeO_2 is observed at the wave propagation along the [1 0 0] and [0 0 1] direction, absorption coefficients being 19 dB/cm and 9 dB/cm. The obtained structural data indicate that this absorption anisotropy well correlates with the anisotropy of anharmonic components of thermal vibrations of Te atoms. These components are maximum in the [1 1 0] direction and are equal to zero in the [0 0 1] direction.

Deformation electron density maps were constructed in order to locate the lone electron pair of Te atom in space. The complexity of constructing these maps consists in the fact that it is necessary to separate anisotropy of thermal atomic vibrations and the asymmetry in the spatial distribution of valence electrons of these atoms in the structure. Parameters of thermal vibrations of these atoms were refined from high-angle reflections that are free from the influence of external valence electrons. Fig. 9 shows the deformation electron density map passing through a density maximum of a lone electron pair. The assumptin advanced earlier in the literature that a lone electron pair of Te atom should be located at

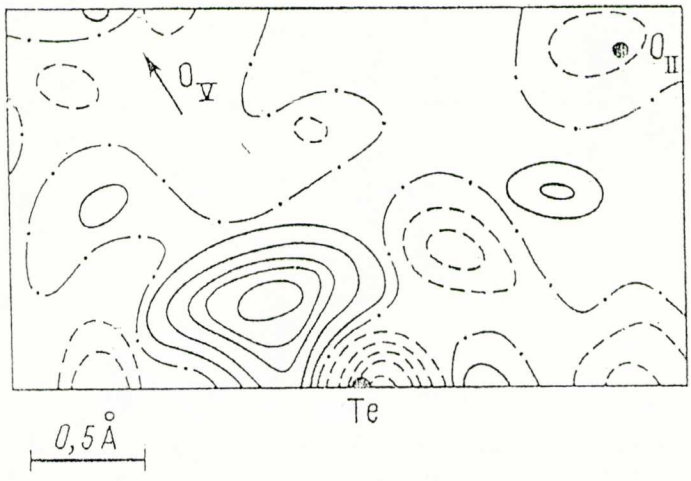

Fig. 9. Structure of α–TeO_2. Location of a lone electron pair of Te atom.

the equator of a trigonal bipyramid at the position of a missing oxygen vertex (on the two-fold axis), proved to be wrong. The lone electron pair of Te atom is represented by two peaks (in Fig. 8 the second peak related by the two-fold axis, is not shown) on the lines of interaction of Te atom with oxygen atoms from the second coordination sphere.

The above examples show that precisional structural studies make it possible to determine the structure parameters that correlate with properties of crystals that are valuable for solid state physics and technology. Modification of the properties of crystalline materials and search for new compounds with desired properties can be performed only on the basis of fundamental knowledge of the atomic structure of matter.

Abstract

The advances in the techniques of accurate crystal structure analysis make it possible to establish regular correlations between the atomic structure and physical properties of crystalline materials. Modern diffraction methods ensure not only a high accuracy of the determination of aotmic coordinates, but also provide reliable data on atomic thermal motion, with allowance for both *anharmonic* and deviations from the *harmonic* law. Structural analysis yields atomic mechamism of phase transitions in crystals, as well as qualitative characteristics of isomorphous replacements in samples and the degree of structure perfection of a particular single crystal.

The paper presents results of structural studies of high-temperature superconductors, crystals with high ionic conductivity, ferroelectrics and some other crystalline materials.

REFERENCES

1. Methods of structural analysis (Problems of Modern Crystallography Series), Moscow, Nauka Publishers, 1989, 304 p. (in Russian).
2. J. B. Bednorz, K. A. Muller. Z. Phys. B., 1986, 64, 189.
3. V. I. Simonov, L. A. Muradyan, R. A. Tamazyan, O. K. Melnikov, A. B. Bykov, B. K. Vainshtein. Pisma v ZHETF 1988, 48, 5.290.
4. L. A. Muradyan, V. N. Molchanov, R. A. Tamazyan, V. I. Simonov, Physica C, 1989, 162-164, 536.
5. C. Chaillout, J. Chenavas, S. W. Chong, Z. Fisk, M. S. Lehmann, M. Marezio, B. Morosin, J. E. Schirber. M2HTSC Meeting, July 89, Stanford, USA.
6. I. V. Aleksandrov, A. B. Bykov, I. P. Zibrov et al. Pisma v ZHETP, 1988, 48, 449.
7. V. N. Molchanov, L. A. Muradyan, V. I. Simonov. Pisma v ZHETF, 1989, 49, 222.
8. Z. Hiroi, M. Takano, Y. Bando. Physica C, 1989, 158, 269.
9. I. P. Kondratyuk, M. I. Sirota, B. A. Maximov, L. A. Muradyan, V. I. Simonov. Kristallografiya, 1986, 31, 3, 488.
10. B. A. Maximov, L. A. Muradyan, E. A. Genkina, V. I. Simonov. DAN SSSR, 1989, 288, 3, 634.
11. I. P. Makarova, E. E. Riderr, V. A. Sarin, I. P. Alexandrova, V. I. Simonov. Kristallografiya, 1989, 34, 4, 583.
12. I. P. Makarova, L. A. Shuvalov, V. I. Simonov. Ferroelectrics, 1988, III, 79.
13. N. Uchida. J. Apl. Phys., 1972, 43, 2915.
14. V. I. Balakshii, V. N. Parygin, L. E. Chirkov. Physical foundations of acoustoptics. Moscow, Radio i Svyaz Publishers, 1985, 280 (in Russian).
15. I. P. Kondratyuk, L. A. Muradyan, Yu. V. Pisarevskii, V. I. Simonov. Kristallografiya, 1987, 32, 3, 609.
16. International Tables for X-ray Crystallography, Birmingham, Kynoch Press, 1974, 366.